processes

MDPI

Article

Investigation on Impact Strength of Friction Stud Welded AA6061-B_4C Composite/AISI 1030 Steel Joints in Inert Gas Atmosphere

Navasingh Rajesh Jesudoss Hynes [1,*], Selvaraj Raja [1], Ramakrishnan Tharmaraj [2], Michael Brykov [3] and Antoaneta Ene [4,*]

[1] Department of Mechanical Engineering, Mepco Schlenk Engineering College, Sivakasi 626005, Tamilnadu, India
[2] Department of Mechanical Engineering, SRM Institute of Science and Technology, Ramapuram Campus, Chennai 600089, Tamilnadu, India
[3] Physics and Engineering Department, Zaporizhzhya Polytechnic National University, Zaporiz'ka Oblast', 69600 Zaporizhzhya, Ukraine
[4] INPOLDE Research Center, Department of Chemistry, Physics and Environment, Dunarea de Jos University of Galati, 47 Domneasca St., 800008 Galati, Romania
* Correspondence: findhynes@yahoo.co.in (N.R.J.H.); antoaneta.ene@ugal.ro (A.E.)

Abstract: A more contemporary variation of the friction welding procedure, friction stud welding, is promising for military, space, automotive and naval applications. The joining of steel/aluminium matrix composite joints has been crucial in many of these contemporary applications. In all of these applications, the strength of the dissimilar joint is a critical consideration. Heat-affected zones arise because of the heterogeneous temperature distribution and change in thermal characteristics, which weaken the strength of the joints between different materials. The presence of oxygen in the weld interfacial region of the dissimilar joint is detrimental to its strength and integrity. Hence, a new method that can strengthen the dissimilar joint is adopted in the current work. In the friction stud-welding machine, an additional set up is integrated for providing an inert atmospheric condition during the welding process. Microstructural analysis shows that an inert atmosphere is helpful to get rid of oxygen at the interface and it increases joint efficiency. The results show that the impact strength of AA6061-B_4C composite/AISI 1030 steel joints tends to increase in the argon inert atmosphere from 14% to 28%.

Keywords: friction stud welding; dissimilar materials; inert atmospheric condition; mechanical properties; scanning electron microscope

Citation: Hynes, N.R.J.; Raja, S.; Tharmaraj, R.; Brykov, M.; Ene, A. Investigation on Impact Strength of Friction Stud Welded AA6061-B_4C Composite/AISI 1030 Steel Joints in Inert Gas Atmosphere. *Processes* **2022**, *10*, 2052. https://doi.org/10.3390/pr10102052

Academic Editor: Chin-Hyung Lee

Received: 5 August 2022
Accepted: 7 October 2022
Published: 11 October 2022

1. Introduction

Aluminium (Al) alloys are utilised as structural materials in a variety of industries, including automotive, aircraft, and railway. There is a necessity in the automobile engineering field to weld a earthing pin made of steel to car body made of aluminium matrix composite. Current engineering applications necessitate materials that are stronger, lighter, and less expensive. These materials should be developed with superior mechanical qualities, such as a high strength-to-weight ratio, for aerospace and automotive applications [1,2]. In the past, welding was used to join two metals of the same type, whereas fasteners were used to unite metals of different types. Friction stud welding is an engineering advancement that produces welds between various metals without the use of melting or fillers. Friction stud welding does not use electricity to generate heat; instead, as the name implies, friction is used. Dissimilar metal welding has drawbacks to arc welding, such as intermetallic phase types. Traditional and natural welding procedures cannot be utilised to join different metals because of this. Over the last two decades, friction welding technologies have shown promise in the welding of dissimilar metals [3].

Several investigators used a friction welding machine to fuse dissimilar materials by altering process parameters such as rotational speed (RS), friction pressure (FP), friction time (FT), forging pressure (FGP), and forging time (FGT). Friction welding machines have been used to join titanium to nickel, bronze to steel and brass to copper, using a choice of intermediate materials as interlayers [4]. The applicability of a friction welding machine to join Al to steel and Al to ceramic was performed, and the challenges encountered while combining these different materials were investigated [5]. To produce a satisfactory weld quality, ceramics were welded to metals with the use of friction welding equipment by altering the different process parameters [6]. AA 6063 and AISI 1030 steel materials were fused together using a friction stud welding machine at different process parameters, such as RS, FP, FT, FGP, and FGT. Ultrasonic testing was used to analyse the mechanical properties of the welded specimen [7]. Al was used as an interlayer in friction stud welding of Al_2O_3 and steel. The thermomechanical phenomena were studied using a computational model based on finite elements [8]. To join different Al and mild steel, a friction stud welding procedure was used. The process parameters were adjusted to investigate the strength of the welded specimens. The welded specimen's strength was determined by the RS, FT, and axial shortening distance [9].

The numerical simulation approach is particularly useful for estimating the stress fields and distribution of temperature of the friction welding process. Using finite element software, the friction stud welding of ceramic to the metal with the interlayer was numerically simulated. As a result of the increased interlayer thickness, the researchers noticed a decrease in the heat-affected zone [10]. Some researchers examined numerical simulations of friction stud-welded dissimilar materials, such as alumina to AA 6063 and MMCs to steel joints [11,12]. The thermal fields play a critical role in obtaining a satisfactory welded specimen during the friction stud welding procedure. Using finite element methods, a heat flow model of Al and mild steel during friction stud welding was created [13–16]. Because of the larger plastic deformation throughout the procedure, mechanical properties are affected and microhardness at the interface increases. Microstructural investigation shows dynamically recrystallized grains closer to the interfacial area [17]. Raturi et al. investigated the FSW of 6061-T6 Al and 7075-T651 Al alloys [18]. Tensile failure of the joints was detected from the base metal of the advancing side, according to the researchers (AA6061-T6). Furthermore, with a scanning electron microscopy examination the presence of multiple dimples was revealed in the fracture surfaces, indicating ductile failure of the joints subject to tensile loading. The influence of tool offset and material location during FSW of AA6061-T6 and AA7075-T6 alloys was investigated by Cole et al. [19]. They found that putting the AA7075-T6 on the retreating side with the tool offset into the retreating side raised the tensile strength of the joined specimen because the amount of AA7075 alloy in the welded nugget was increased. In an experiment using the finite element approach, Tang and Shen investigated the influence of preheating with an electric arc heater on material flow and temperature distribution during FSW between Al alloy and steel by experimental and numerical approaches [20]. They claim that preheating minimises the temperature difference between the welded material, which increases material flow and strength. Friction stir welding, according to Ji et al. was beneficial in improving the mixing degree of Mg/Al alloys and breaking partial IMCs into particles, thereby boosting joint strength [21]. Zinc was introduced as a buffer at the interface to enhance the desirable mechanical properties [22]. Hynes et al. joined AA6061 to MgAZ31 B in an in-house modified milling machine by changing the offset [23]. The presence of oxygen and unwanted inclusions were noticed [24–26]. Such findings were further reported as well [27,28]. Interlayers were employed to overcome challenges such as oxygen inclusion in the interfacial region [29–33]. Seli et al. [34] investigated the friction welding of Al_2O_3–steel, using an Al interlayer and found the effect of interlayers keeping the rotational speed constant.

Oxidization quickly occurs when fusion welding is conducted in a natural environment and can contribute to both slag inclusion and porosity in the weld, which will significantly reduce its intensity. In order to overcome these issues, we have to eliminate the presence of

oxygen by coating the solder pool with an inert gas. Inert gases such as argon or nitrogen may be used for this. In this work, argon gas was used as the shielding gas. The application of an inert atmospheric shield would increase the consistency of the weld and enhance the deposit's properties.

2. Materials and Methods

2.1. Selection of Materials

The aluminium 6061 alloys are mainly used in the application of the automobile and aeronautical industries. Due to its good strength, lightweight and better corrosion properties, 6061-T6 aluminium alloy (AA) is commonly used in aircraft, protection, automobiles and marine areas. AA6061 is a heat-treatable alloy of medium-to-high strength. While it has decreased strength in the weld region, it has very good corrosion resistance and very good weldability. It has medium strength for fatigue. In rail coaches, truck frames, shipbuilding, bridges, and military bridges, and aerospace applications such as helicopter rotor skins, tubes, pylons and towers, transport, rivets and motorboats, AA6061 is usually used for heavy-duty structures. Tables 1 and 2 list the chemical composition and mechanical properties of AA6061 in a normal atmosphere.

Table 1. Chemical composition of AA6061 [33].

Element	Weight %
Al	97.6
Zn	0.25
Cu	0.15
Mn	0.15
Ti	0.15
Mg	0.8
Fe	0.7
Si	0.4
Cr	0.04
Others each	0.05
Others total	0.15

Table 2. Mechanical properties of AA6061 [33].

Properties	Value
Density (kg/m^3)	2700
Tensile strength (MPa)	310
Poisson's ratio	0.33

Boron carbide (B_4C) ranks third behind diamond and cubic B_4C as one of the hardest materials known. It is the hardest material produced in terms of tonnage. B_4C powder is used as an abrasive in polishing and lapping applications because of its elevated hardness, and also as a loose abrasive in cutting applications such as water jet cutting. It can also be used on diamond equipment for dressing. Ceramic tooling dies, precision toll components, evaporating boats for measuring materials, mortars and pestles are other applications. The AA6061 reinforced with B_4C is shown in Table 3 and the properties of B_4C are shown in Table 4 in a normal atmosphere.

Table 3. The composition of boron carbide reinforces the AA6061 composite.

Element	Weight %
AA6061	95
B_4C	5

Table 4. Properties of B_4C [35].

Properties	Value
Density (g/cm^3)	2.33–2.55
Tensile strength (MPa)	261
Coefficient of thermal expansion (/°C)	3.2×10^{-6}
Modulus of elasticity (GPa)	362

AISI 1030 steel is known as medium-carbon steel, and in the as-rolled state, has moderate strength and hardness. Via cold practice, it can be hardened and reinforced. It has decent machinability, ductility and reasonable potential for welding as well. For manufacturing machinery components, AISI 1030 carbon steel is suitable. The chemical compositions and mechanical properties of AISI 1030 steel in a normal atmosphere is shown in Tables 5 and 6.

Table 5. Chemical composition of AISI 1030 steel [7].

Element	Weight %
Mo	0.50
C	0.30
Mn	0.80
Si	0.75
Ni	1.00
Cr	11.50
Fe	Remaining

Table 6. Mechanical properties of AISI 1030 steel [36].

Properties	Value
Hardness (HB)	126
Tensile strength (MPa)	463.7
Yield strength (MPa)	341.3
Elongation (%)	31.2

2.2. Friction Stud Welding Machine

The friction stud welding system was developed in the present work by modifying the standard lathe for a general purpose (Type A141, PSG, Coimbatore, India). The main modifications made were the installation of an effective braking system and replacement of compound rest by stud-holder assembly. Welding time, rigid clamping, axial strength, forging pressure and immediate stopping of the spinning object are the essential parameters influencing friction stud welding.

2.3. Friction Stud Welding in an Inert Gas Atmosphere

In the friction stud welding unit, the schematic representation of argon shielding is shown in Figure 1. This fabricated friction stud welding machine was developed through certain modifications performed on a lathe. Welding time, rigid clamping, axial strength, forging pressure and instant stopping of moving artefacts are the critical parameters involved in friction stud welding. Thus, an effective brake device was arranged by means of a simple band brake for instant stopping of the spinning object kept in the chuck. A belt was wound around the brake drum, whose one side was attached to a fixed end and the other side was attached to a movable end. The fixed end was the slacking side and the movable end was the tight side. A lever arrangement was provided to apply less effort while actuating the brake. Using a limit switch, the motor power is cut off simultaneously while the brake lever is actuated.

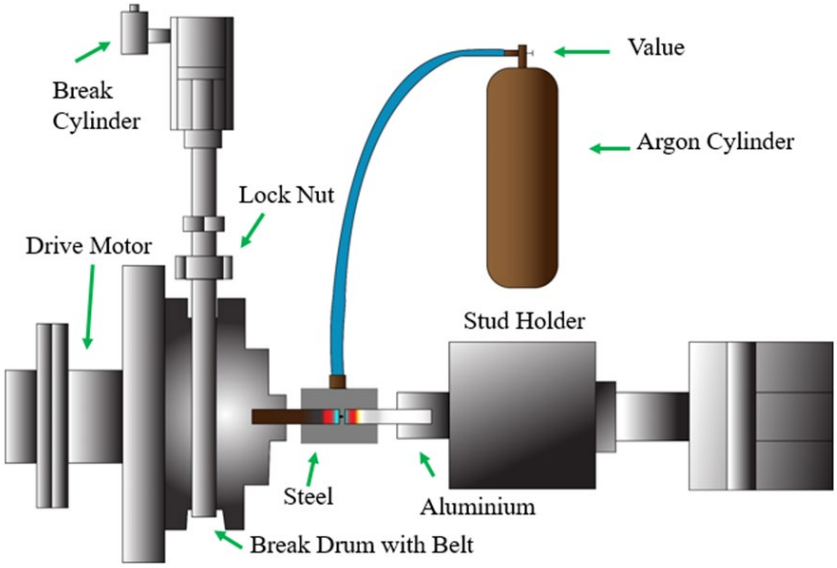

Figure 1. Schematic representation of argon shielding in friction stud welding.

A pneumatic circuit was introduced to deliver uniform axial and forging pressures to the stud against the rotating object in the chuck. For rigid clamping of the stud, a stud holder was fabricated. The stud was screwed into a Morse taper which was fitted in the front end of the stud holder. The front end of the stud holder was machined to suit the Morse taper. The rear end of the stud holder was machined to suit the rod end of the pneumatic cylinder. At the bottom of the stud holder, two holes were drilled and tapped so that it was fastened to the sliding plate with bolts. The sliding plate slides in the guideways. The guideways were fastened to a base plate by means of four Allen screws. The base plate which contains the stud holder assembly and the pneumatic cylinder replaced the compound rest of the lathe. The process parameters were controlled using a programmable logic controller.

2.3.1. Experimental Arrangement for Friction Stud Welding in an Inert Gas Atmosphere

In this work, argon gas was used as the shielding gas. The experimental arrangement for friction stud welding in an inert gas environment is shown in Figure 2.

2.3.2. Preparation of Specimen

Experiments were performed on a direct drive friction stud welding system mounted on a programmable logic controller. Figure 1 shows the schematic representation of the structure for friction stud welding. By machining AISI 1030 steel rods up to 12 mm in diameter and 45 mm in length, samples of AISI 1030 steel were prepared. AA 6061 stud samples of equal diameter and length, with a 1.75 mm thread as a pitch, were prepared as shown in Figure 3. The successful friction stud welded AA 6063/AISI 1030 joints are shown in Figure 4. To carry out microstructural analysis, friction stud welded joints were cut vertically to the surface of the joint. Mechanical polishing was then done with different grades of emery papers. Then, they were etched with ferric chloride solution. The specimens prepared for microhardness determination and microstructural analysis are shown in Figure 5.

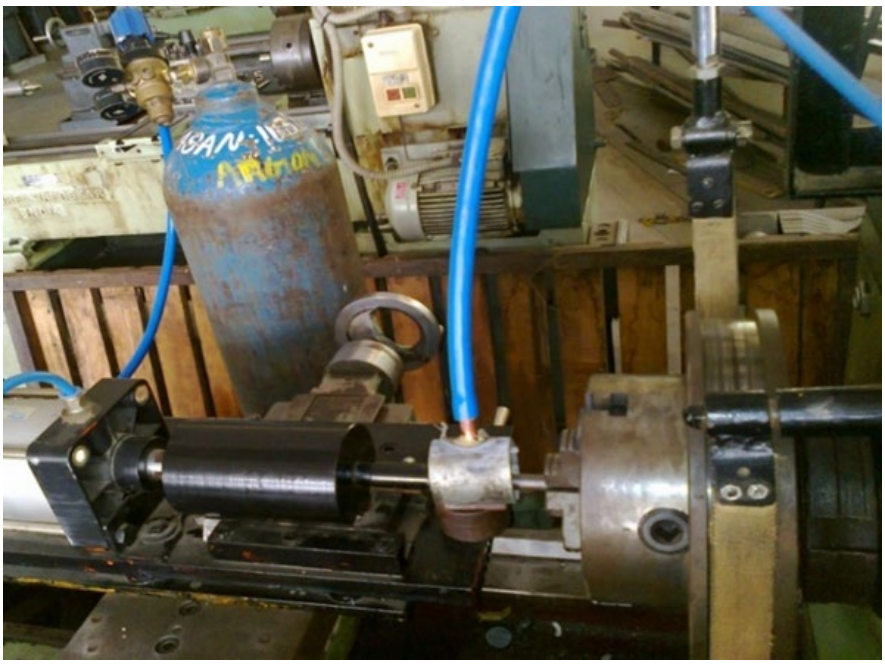

Figure 2. Experimental arrangement for friction stud welding in an inert gas atmosphere.

Figure 3. AA6061-5% B_4C/AISI 1030 steel samples.

Figure 4. Friction welded AA6061-5% B_4C/AISI 1030 steel joints.

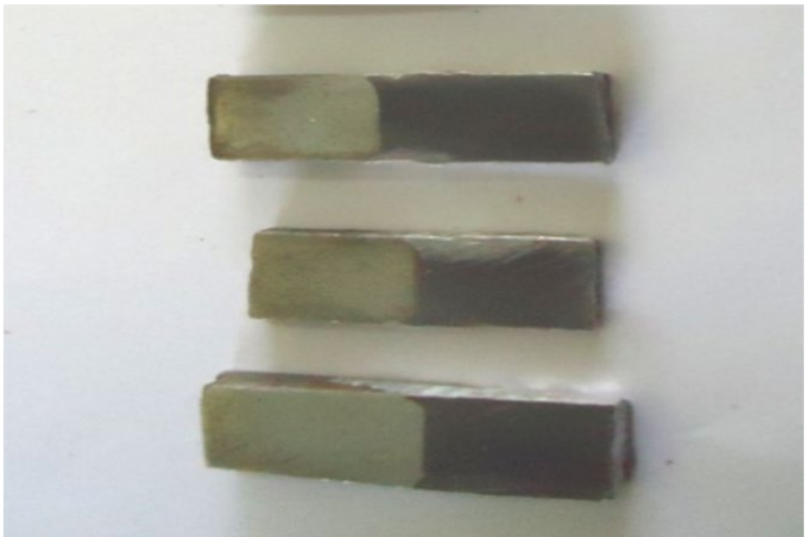

Figure 5. Prepared microstructural research specimens.

2.4. Plan of Experiments

In order to analyse the effect of argon shielding, processing conditions such as rotational speed, friction time, and friction pressure were taken into consideration. During the experimentation, friction time and friction pressure were retained, while the rotational speed was varied: 800, 1150 and 1600 rpm. At first, experimental runs were conducted under normal conditions that were without shielding. Afterwards, the experimental runs were repeated with argon shielding in an inert atmosphere. These experimental plans are tabulated in Table 7.

Table 7. Plan of experiments.

Rotational Speed (rpm)	Friction Time (s)	Friction Pressure (MPa)	Atmospheric Conditions
800	6	600	Normal atmosphere
1150	6	600	
1600	6	600	
800	6	600	With argon shielding
1150	6	600	
1600	6	600	

2.5. Mechanical Testing and Microstructural Analysis Testing

Mechanical testing was conducted in order to assess the impact strength of the welded joints. Using the Charpy effect measurement device, this was carried out at room temperature. Impact test samples measuring 10 × 7.5 × 50 mm were prepared with a 2 mm deep 'V' notch and a 450 groove in line with the ASTM A370 requirements. The specimen perpendicular section was made to the weld surface for microstructural inspection, and mechanical polishing was performed using emery papers accompanied by ferric chloride solution etching.

Using SEM (Hitachi, SU1510—Chiyoda City, Japan), EDX analysis, and microhardness measurement for microstructural evaluation, the prepared specimen was investigated. The Vickers hardness tester was used in order to measure the microhardness variations across the welded joint. Indents were made for a load of 5 kg and a holding time of 20 s on the welded specimen. The indenter was then removed from the surface of the sample and used to calculate the indentation dimensions using an optical microscope.

3. Results and Discussion

3.1. Microhardness Measurement

Figure 6 shows the microhardness distribution of AA6061-5%B_4C/AISI 1030 steel dissimilar friction stud welded joint, processed under normal atmospheric conditions. Figure 7 shows the microhardness distribution of a AA6061-5%B_4C/AISI 1030 steel joint processed under argon shielding. The microhardness value was high at the weld interface in both instances and it changed when moving away from the base materials. On the steel side and on the AA6061-5%B_4C side, which is the same as that of the parent products, it decreases and achieves constant value. The presence of diverse zones in the heat-affected area of the welded joint is indicated by a shift in the hardness values.

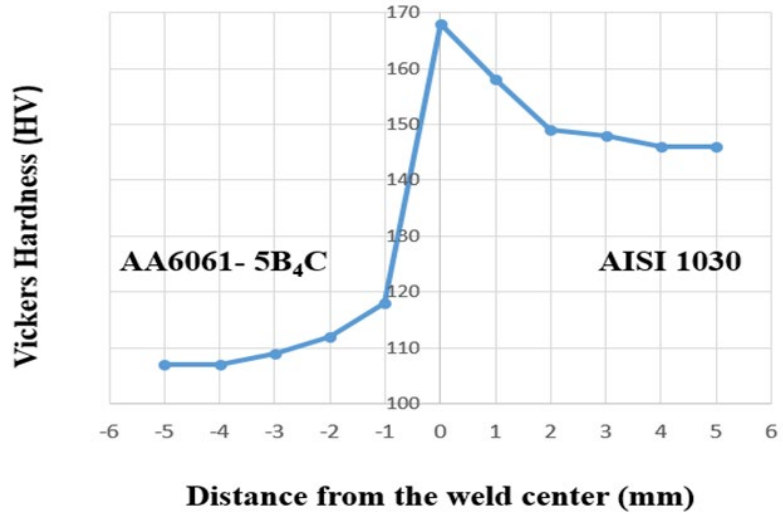

Figure 6. Microhardness distribution of AA6061 - 5%B_4C/AISI 1030 friction welded joint processed under normal conditions.

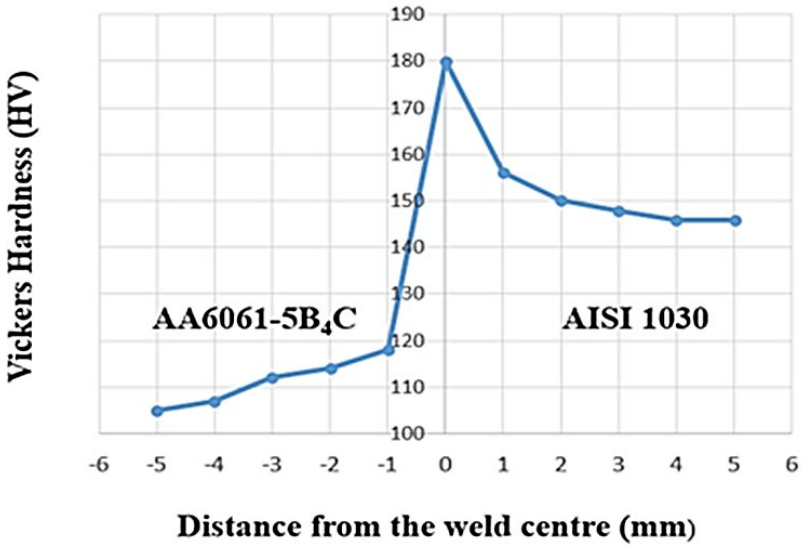

Figure 7. Microhardness distribution of AA6061-5%B_4C/AISI 1030 friction welded joint processed in an inert atmosphere.

In the interfacial region, due to increased heat input at the friction point, the microstructural analysis suggested increased plastic deformation. Plastic deformation reduces the grain size. This can contribute to hardening inside the welding interface. The value of hardness is, therefore, in the high interfacial region. Dynamic recrystallization has

taken place in the fully plasticized deformed area. The hardness value increases after this recrystallization region due to the job hardening caused by the applied upsetting load during the upsetting stage. The impacts of frictional heat and work hardening are slight a little farther away from this area. Therefore, the hardness values are closer to those of the base metal.

The microhardness values measured around the welded joint were shown to demonstrate the distribution of microhardness measured perpendicular to the weld joint interface in Figures 6 and 7. On the AISI 1030 side, the microhardness measured near the weld centre was around 150 HV and it gradually decreased to 148 HV. Similarly, the microhardness on the AA6061-5%B_4C side of the fully plasticized area was 120 HV and progressively decreased to 108 HV. Here, the minimum microhardness value was close to that of the parent material as it stays in the unaffected area.

Argon shielding restricts metal oxide for motion when compared with normal atmospheric conditions [9]. In a fully plasticized zone, it was measured that the maximum hardness value was 168 Hv for the friction stud welded component joined at normal atmospheric conditions. However, in an inert atmosphere the microhardness value was 180 Hv because of the absence of metal oxides. The increase in the interface is due to the deformation of plastic induced by the disturbing strain caused during the welding of the friction stud. According to the Hall–Petch equation, fine grains that are dynamically recrystallized increase both the hardness value and the joint power. A dip in the hardness value indicates the presence of the partially deformed region. The hardness value was the same as that of the parent material in the third unchanged region, where it was further reduced and then a set of simple principles was adopted.

3.2. Scanning Electron Microscope Analysis

The interfacial area of the friction stud welded joints was defined using SEM to better understand the bonding mechanism. Figures 8 and 9 show the scanning electron micrographs of welded joints in normal conditions, and inert atmosphere, respectively. The creation of new phases, the presence of oxides, and the diffusion of elements through the interface are obvious from the micrograph. The AA6061-5%B_4C side consists of porous oxides as well as intermetallic compounds. It was noted that, apart from the welding interface, iron oxide particles were drawn into the AA6061-5%B_4C. In all-welded samples near the interface, the completely plasticized deformed zone containing dynamically recrystallized grains appeared (Figure 8) via electron microscopy; in the dynamically recrystallized area, very fine recrystallized grains are observed.

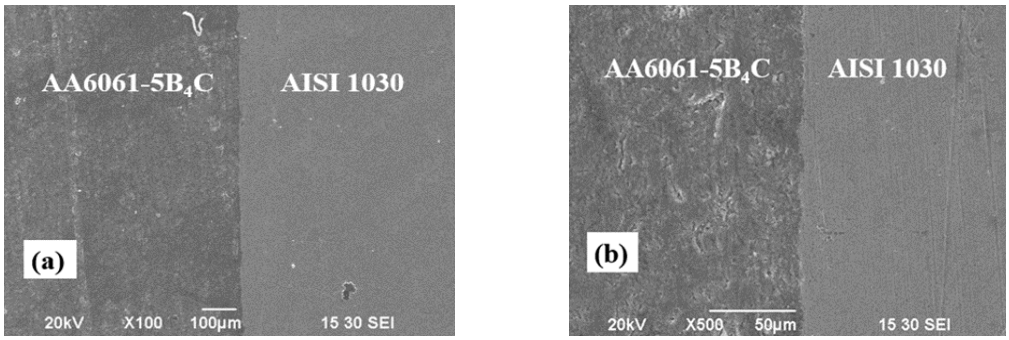

Figure 8. Scanning electron micrograph at the interface of the welded joint at the normal condition at 1600 rpm, (**a**) at a magnification of 100× and (**b**) at a magnification of 500×.

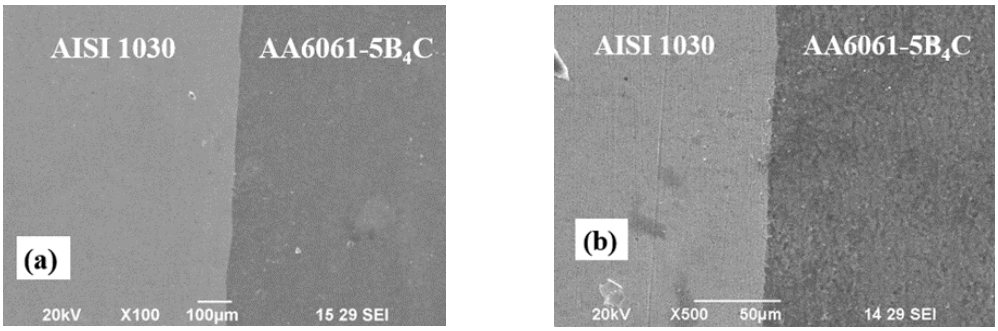

Figure 9. Scanning electron micrograph at the interface of the welded joint processed in an inert atmosphere, (**a**) at a magnification of 100× and (**b**) at a magnification of 500×.

3.3. Energy-Dispersive X-ray Analysis

Energy-dispersive X-ray analysis (EDX) in the section of the friction stud welded interface was carried out using optimum parameters. The results of the EDX joint interface analysis processed under normal conditions without argon are shown in Figure 10.

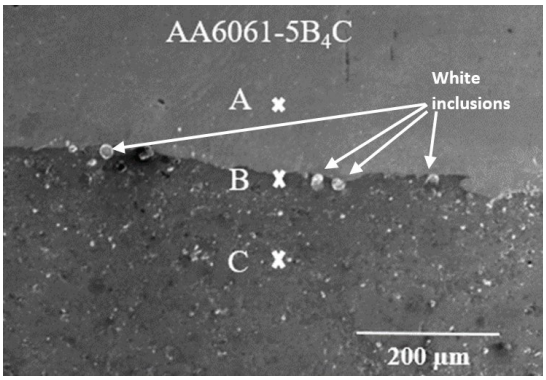

Figure 10. Three-point EDX study of AA6061-5%B_4C joint sample friction stud welded under normal conditions.

3.3.1. EDX Analysis of Specimen Welded at Normal Conditions

Figure 10 shows EDX analysis at three points of the AA6061-5%B_4C friction stud welded specimen under normal conditions. Figures 11–13 show the EDX analysis spectrum at points A (AA6061-5%B_4C side), B (interface) and C (AISI 1030 steel side) in the AA6061-5%B_4C joint specimen. In Tables 8–10, A, B and C are given after EDX analysis results. The presence of a high content of oxygen suggests that the weld zone contains thick iron oxide. Owing to frictional heating, the material becomes viscous and there is also diffusion of iron atoms that join the interface by taking oxygen from the atmosphere.

Metal oxides are formed in the interface region of the AISI 1030/AA 6061-5%B_4C joint. A thin, discontinuous inter-metallic layer is found at the welding interface because of the inter-diffusion between iron and aluminium. The EDX analysis gives 37.15% Al, 7.85% Fe, and 28.90% O within the interfacial zone. The presence of the intermetallic compound Fe_3Al correlates to this composition.

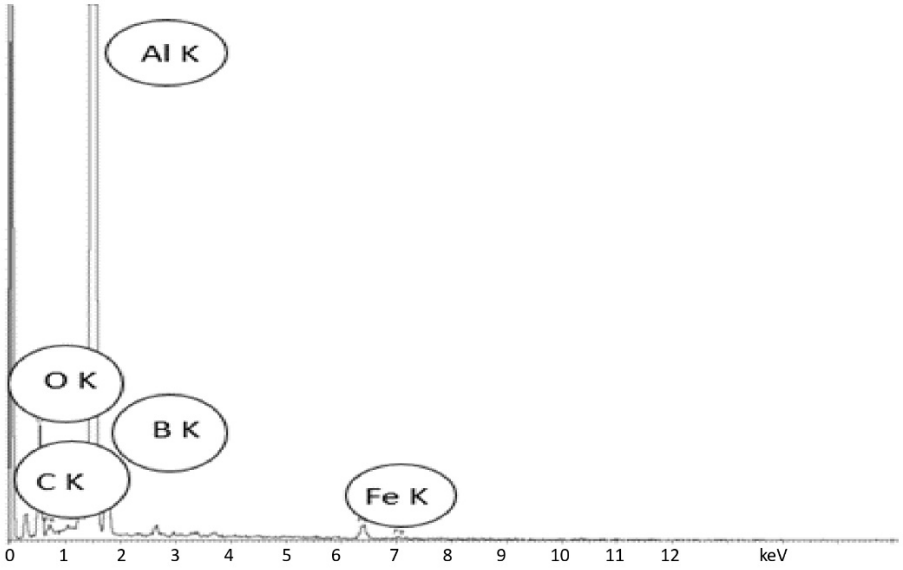

Figure 11. EDX analysis spectrum at point A in specimen welded at normal conditions.

Table 8. EDX quantitative analysis data at point A in specimen welded at normal conditions.

Element	Weight %	Atomic %
O K	23	33.98
C K	0.8	0.78
Al K	67.63	59.24
B K	5.67	4.77
Fe K	2.89	1.22

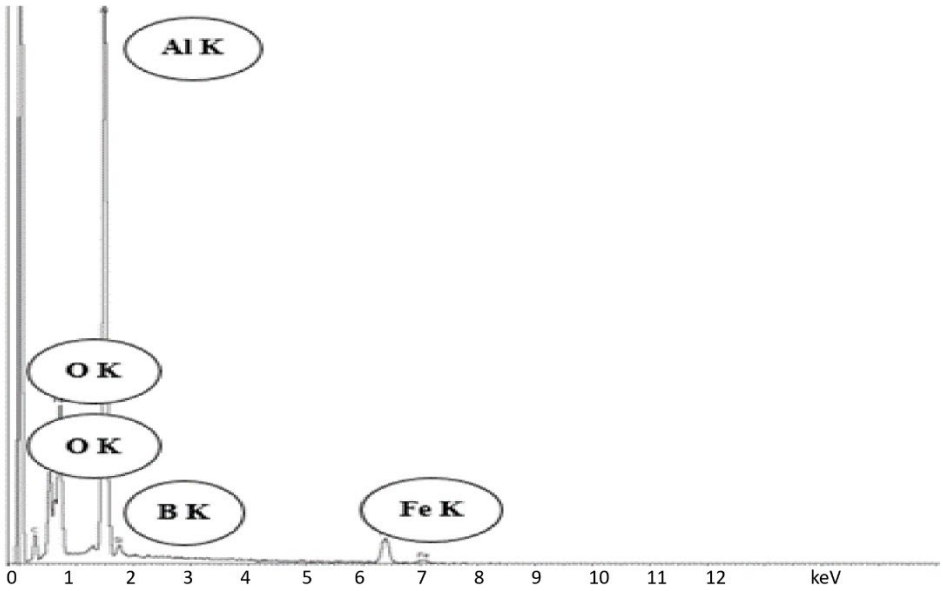

Figure 12. EDX analysis spectrum at point B in specimen welded at normal conditions.

Table 9. EDX quantitative analysis data at point B in specimen welded at normal conditions.

Element	Weight %	Atomic %
O K	25.19	38.46
C K	28.9	33.13
Al K	37.15	25.24
B K	0.91	0.59
Fe K	7.85	2.58

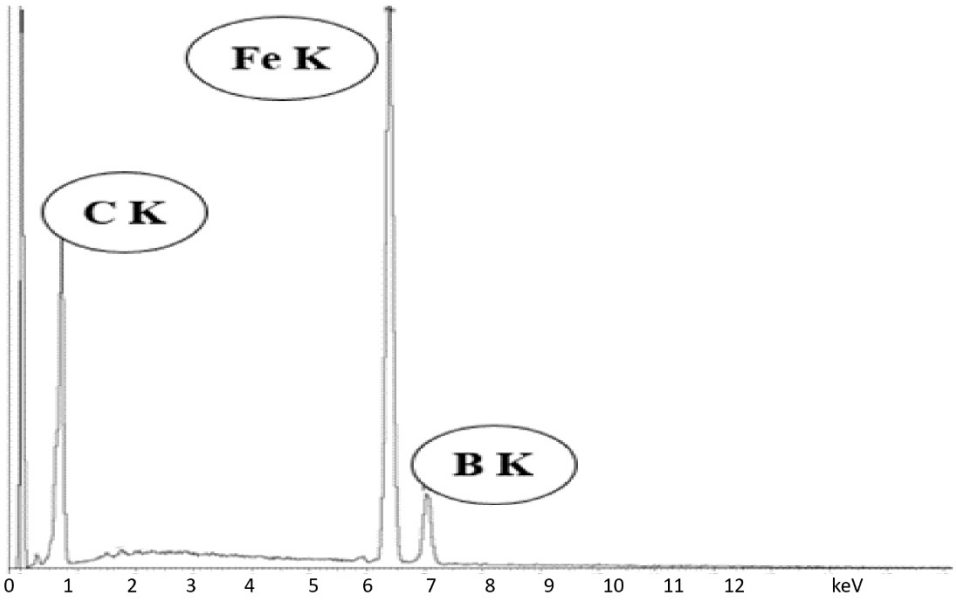

Figure 13. EDX analysis spectrum at point C in specimen welded at normal conditions.

Table 10. EDX quantitative analysis data at point C in specimen welded at normal conditions.

Element	Weight %	Atomic %
C K	4.66	18.47
B K	0.34	0.57
Fe K	95	80.96

3.3.2. EDX Analysis of Specimen Welded at Inert Atmosphere

Figure 14 shows EDX analysis at three points of the AA6061-5%B_4C friction stud welded specimen in the inert atmosphere of argon shielding. AA6061-5%B_4C appears dark grey and AISI 1030 steel appears bright. Figures 15–17 show the EDX analysis at points A, B and C of the AA6061-5%B_4C friction stud welded specimen in the inert atmosphere of argon shielding. Tables 11–13 reveals the respective EDX analysis data. EDX analysis of the interfacial region reveals the presence of 50.23% Al and 46.70% Fe by weight. This composition substantiates the presence of $FeAl_2$.

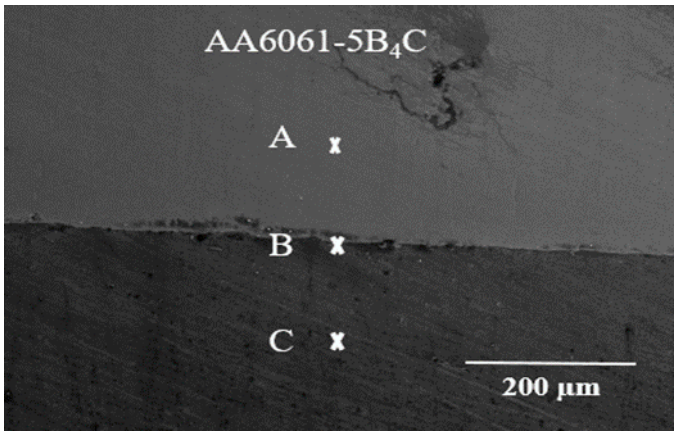

Figure 14. EDX analysis at three points of the AA6061-5%B_4C friction stud welded specimen in inert atmosphere of argon shielding.

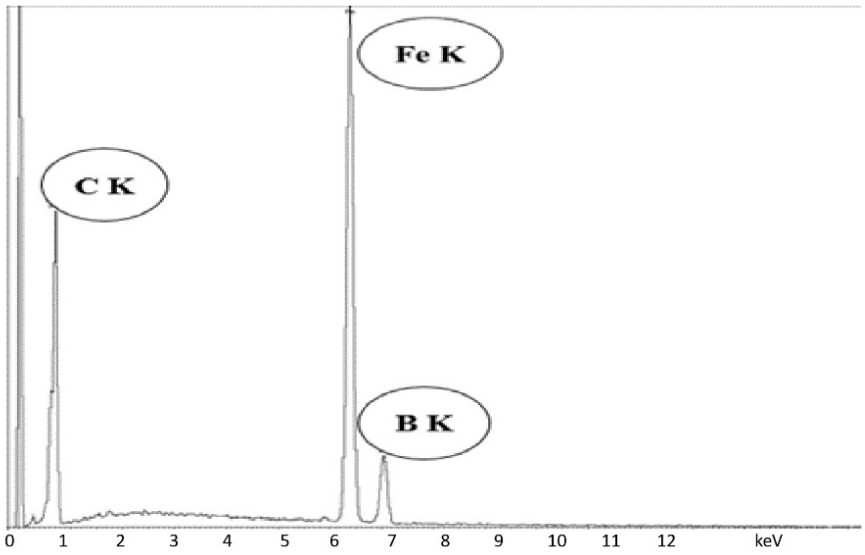

Figure 15. EDX analysis spectrum at point A in specimen welded in inert conditions.

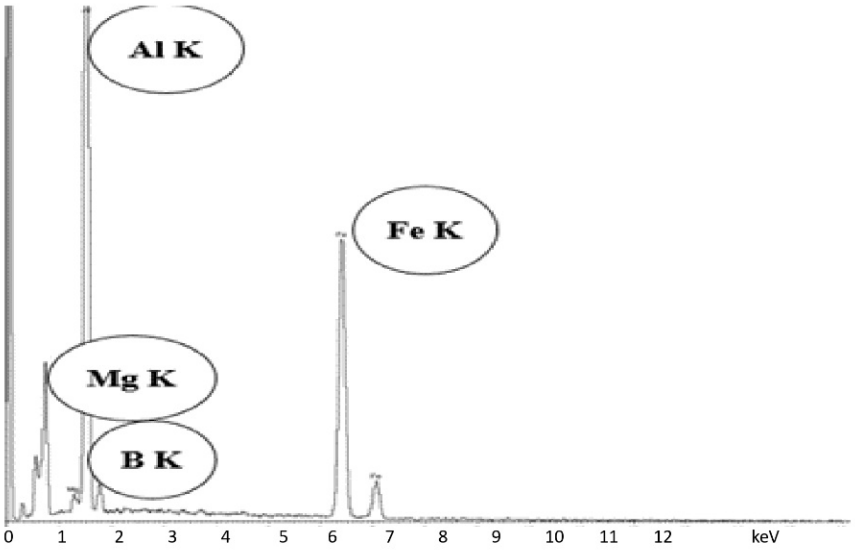

Figure 16. EDX analysis spectrum at point B in specimen welded in inert conditions.

Table 11. EDX analysis quantitative at point A in specimen welded in inert conditions.

Element	Weight %	Atomic %
C K	3.44	14.17
B K	0.43	0.76
Fe K	96.12	85.07

Table 12. EDX quantitative analysis data at point B in specimen welded in inert conditions.

Element	Weight %	Atomic %
Mg K	1.02	1.49
Al K	50.23	66.18
B K	2.06	2.61
Fe K	46.7	29.93

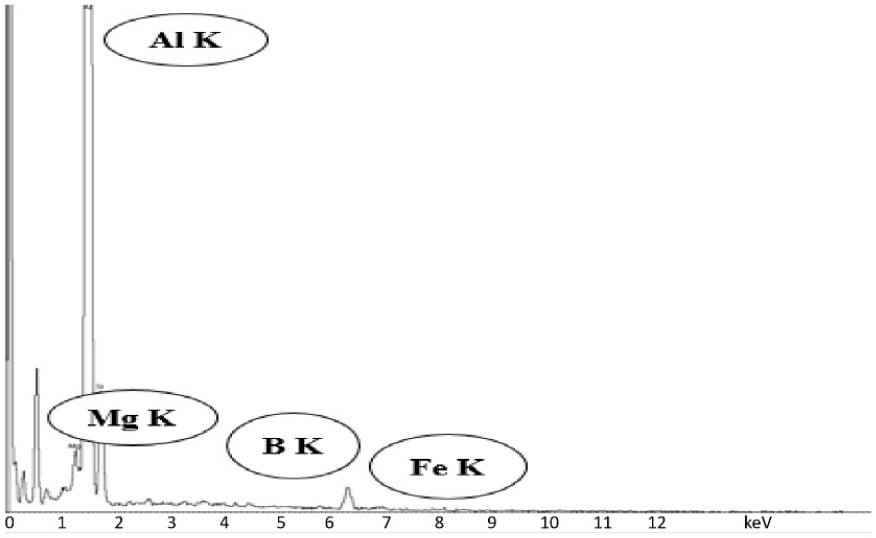

Figure 17. EDX analysis spectrum at point C in specimen welded in inert conditions.

Table 13. EDX quantitative analysis data at point C in specimen welded in inert conditions.

Element	Weight %	Atomic %
Mg K	1.15	1.31
Al K	86.07	87.97
B K	9.06	8.89
Fe K	3.72	1.83

3.3.3. Intermetallic Phases at Interfaces

The development of brittle intermetallic stages is unavoidable and the strength of the steel joints of the AMC/AISI 1030 was reduced. Intermetallic compound formulation depends on the peak temperature and the thermal period of the process at the interface of the joint. Embrittlement of the joining zone can be observed along with the step forming [37]. To optimise the strength and strength of different joints, the creation of intermetallic phases should be limited to a minimum scale. Thus, the main factors to be considered are the total heat input and the width reduction of the heat-affected area. In the joint interfacial region, high thermal gradients and the resulting rapid cooling have been found to be capable of greatly limiting the formation of intermetallic phases. It is evident that at least five stable intermetallic compounds are probable in which, two intermetallic compoundsrich in iron (FeAl and Fe_3Al), two intermetallic compounds rich in aluminium ($FeAl_3$ and Fe_2Al_5) and

another intermetallic compound with an equal amount of iron and aluminium ($FeAl_2$). When welded in the interfacial region of the sample under normal conditions, the EDX analysis gives 37.15% Al, 7.85% Fe, and 28.90%. This composition in the interfacial region of the specimen welded to the inert atmosphere.

3.4. Impact Strength

The impact strength of the friction stud welded component can be equated with the strength of the parent metal. The impact strength of the friction stud welded AISI 1030/AMC dissimilar joint was found to be of much lower value in the present work compared with the base metal. The effect of process parameters such as rotation speed in the inert atmosphere and axial shortening distance on the impact strength of the friction stud welded components were investigated by conducting experimental runs. By comparing the results obtained under normal atmospheric conditions, Table 14 demonstrates the effect of argon shielding on axial shortening (AS) and impact strength (IS).

Table 14. Tabulation of experimental results.

Processing Conditions			Normal Atmosphere		With Argon Shielding		Effect of Argon Shielding	
RS (rpm)	FT (s)	FP (MPa)	IS (kg/mm^2)	AS (mm)	IS (kg/mm^2)	AS (mm)	% of Decrease in AS	% of the Increase in IS
800	6	600	180	3.64	200	3.24	10.99	14.29
1150	6	600	193.33	6.05	240	5.71	9.34	33.34
1600	6	600	280	6.97	320	6.36	16.76	28.57

The notched Charpy impact test was performed on the impact tester in compliance with the ASTM E23 standard. Figure 18 compares the impact strengths of the parent metals and welded joint in normal atmospheric conditions and in an inert atmosphere (with Argon shielding). Though the impact strengths of welded components were less when compared with that of parent metals, it was evident from Figure 18 that argon shielding tends to increase the impact strength from 25 joules to 35 joules. The impact strength substantially increased from about 14% to 28% for friction welded components processed in an inert atmosphere of argon shielding.

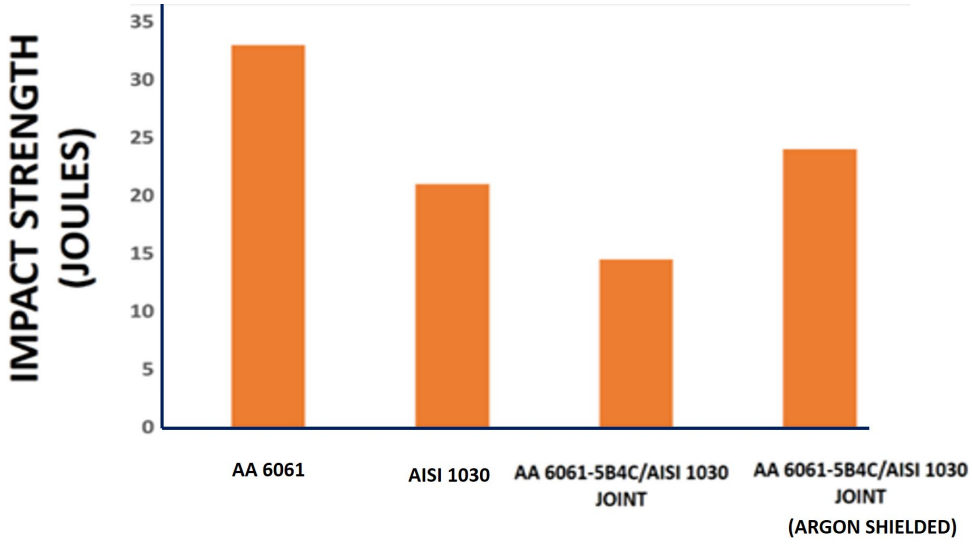

Figure 18. Comparison of impact strength of friction welded joints.

4. Conclusions

Friction stud welding of dissimilar joints made of AA6061-5%B_4C/AISI 1030 steel combinations was made successful in normal conditions and in inert atmospheric conditions. The hardness value increase in the completely plasticized deformed zone in the interfacial area was highlighted by the microhardness profile. This was due to the deformation of plastic produced by disturbing strain. Due to the absence of metal oxides, the microhardness of the friction welded joint processed in the inert atmosphere was 180 Hv. The microhardness of the friction welded joint processed in the inert atmosphere was 180 Hv due to the absence of metal oxides. SEM micrographs reveal the presence of metal oxides near the weld interface of friction stud welded AA6061-5% B_4C/AISI 1030 steel joints processed under normal conditions. EDX analysis shows the tendency for the formation of metal oxides near the interfacial region of the friction welded AA6061-5% B_4C/AISI 1030 steel joints processed under an inert atmosphere in the presence of argon gas is lesser. The presence of intermetallic phases was found in the weld interface using EDX analysis for the friction welded joint processed under normal conditions. The intermetallic compound determined was Fe_3Al. For the friction welded joint processed under an argon atmosphere, there was a tendency for the formation of the $FeAl_2$ intermetallic compound. The presence of $FeAl_2$ increases the microhardness of friction stud welded joints processed under an inert atmosphere. Increasing microhardness boosts the power of the AA6061-5% B_4C/AISI 1030 steel joint as per Hall–Petch's relation. From the experimental findings, it is evident that friction stud welding tends to increase the impact strength in the argon inert atmosphere from 25 joules to 35 joules, a substantial increase from around 14% to 28%.

Author Contributions: Conceptualization and methodology, N.R.J.H. & A.E.; investigation, N.R.J.H. and A.E.; formal analysis, N.R.J.H. and M.B.; writing—original draft preparation, N.R.J.H., S.R.; writing—review and editing, A.E., M.B., R.T. and N.R.J.H. All authors have read and agreed to the published version of the manuscript.

Funding: "Dunarea de Jos" University of Galati, Romania, grant no. 17094, financed by the project "CEREX UDJG 2022", contract no. CNFIS-FDI-2022-0205.

Institutional Review Board Statement: Not applicable.

Informed Consent Statement: Not applicable.

Data Availability Statement: The data that support the findings of this study are available from the corresponding author upon reasonable request.

Conflicts of Interest: The authors declare no conflict of interest.

References

1. Tjong, S.C. Processing and deformation characteristics of metals reinforced with ceramic nanoparticles. In *Nanocrystalline Materials*, 2nd ed.; Their Synthesis-Structure-Property Relationships and Applications; Elsevier: Amsterdam, The Netherlands, 2014; pp. 269–304.
2. Rino, J.J.; Chandramohan, D.; Sucitharan, K.S.; Jebin, V.D. An overview on development of aluminium metal matrix composites with hybrid reinforcement. *Int. J. Sci. Res.* **2012**, *1*, 196–203.
3. Prater, T. Solid state joining of metal matrix composites: A survey of challenges and potential solutions. *Mater. Manuf. Process.* **2011**, *26*, 636–648. [CrossRef]
4. Sassani, F.; Neelam, J.R. Friction welding of incompatible materials. *Res. Dev.* **1988**, *67*, 264–270.
5. Rombaut, P.; De Waele, W.; Faes, K. Friction welding of steel to ceramic. *Sustain. Construct. Des.* **2011**, *2*, 448–457. [CrossRef]
6. Bonte, D.; Derynck, B.; De Baets, P.; De Waele, W.; Faes, K. Friction welding of ceramics to metals. *Sustain. Construct. Des.* **2010**, *1*, 14–20. [CrossRef]
7. Hynes, N.R.J.; Nagaraj, P.; Sujana, J.A.J. Ultrasonic evaluation of friction stud welded AA6063/AISI1030 steel joints. *Mater. Des.* **2014**, *62*, 118–123. [CrossRef]
8. Hynes, N.R.J.; Velu, P.S. Simulation of friction welding of alumina and steel with aluminum interlayer. *Int. J. Adv. Manuf. Technol.* **2015**, *93*, 121–127. [CrossRef]
9. Hynes, N.R.J.; Nagaraj, P.; Sujana, J.A.J. Investigation on joining of aluminum and mild steel by friction stud welding. *Mater. Manuf. Process.* **2012**, *27*, 1409–1413. [CrossRef]

10. Hynes, N.R.J.; Nagaraj, P.; Basil, S.J. Numerical simulation on joining of ceramics with metal by friction welding technique. *Int. J. Mod. Phys. Conf. Ser.* **2013**, *22*, 190–195. [CrossRef]
11. Hynes, N.R.J.; Velu, P.S.; Tharmaraj, R.; Kumar, R. Numerical investigation on friction welding of alumina/AA 6063 T6 joints. *AIP Conf. Proc.* **2016**, *1728*, 205501–205505.
12. Hynes, N.R.J.; Tharmaraj, R.; Velu, P.S.; Kumar, R. Finite element- based simulation on friction stud welding of metal matrix composites to steel. *AIP Conf. Proc.* **2016**, *1728*, 0205561–0205564.
13. Hynes, N.R.J.; Nagaraj, P.; Palanichamy, R.; Arumugham, C.A.K.; Sujana, J.A.J. Numerical simulation of heat flow of friction stud welding of dissimilar metals. *Arab J. Sci. Eng.* **2014**, *39*, 3217–3224. [CrossRef]
14. Hynes, N.R.J.; Nagaraj, P.; Tharmaraj, R. Prediction of thermal profile during friction stud welding of aluminium—mild steel joints. *Int. J. Appl. Eng. Res.* **2015**, *10*, 6107–6110.
15. Hynes, N.R.J.; Tharmaraj, R. Thermal model for heat flow in friction stud welding. *J. Therm. Eng. Appl.* **2015**, *2*, 22–27.
16. Hynes, N.R.J.; Nagaraj, P.; Tharmaraj, R. Thermal analysis on joining of dissimilar metals by friction stud welding. *Adv. Mater. Res.* **2014**, *984–985*, 592–595. [CrossRef]
17. Hynes, N.R.J.; Nagaraj, P.; Sujana, J.A.J. Mechanical evaluation and microstructure of friction welded aluminium-mild steel joints. *Arab J. Sci. Eng.* **2014**, *39*, 5017–5023. [CrossRef]
18. Raturi, M.; Garg, A.; Bhattacharya, A. Joint strength and failure studies of dissimilar AA6061–AA7075 friction stir welds: Effects of tool pin, process parameters and preheating. *Eng. Fail Anal.* **2019**, *96*, 570–588. [CrossRef]
19. Cole, E.G.; Fehrenbacher, A.; Duffie, N.A.; Zinn, M.R.; Fefferkorn, F.E.P.; Ferrier, N.J. Weld temperature effects during friction stir welding of dissimilar aluminium alloys 6061-t6 and 7075-t6. *Int. J. Adv. Manuf. Technol.* **2014**, *71*, 643–652. [CrossRef]
20. Tang, J.; Shen, Y. Effects of preheating treatment on temperature distribution and material flow of aluminum alloy and steel friction stir welds. *J. Manuf. Process.* **2017**, *29*, 29–40. [CrossRef]
21. Ji, S.; Meng, X.; Liu, Z.; Huang, R.; Li, Z. Dissimilar friction stir welding of 6061 aluminum alloy and AZ31 magnesium alloy assisted with ultrasonic. *Mater. Lett.* **2017**, *201*, 173–176. [CrossRef]
22. Boucherit, A.; Fenoel, M.N.A.; Taillard, R. Effect of a Zn interlayer on dissimilar FSSW of Al and Cu. *Mater. Des.* **2017**, *124*, 87–99. [CrossRef]
23. Rajesh Jesudoss Hynes, N.; Vivek Prabhu, M.; Shenbaga Velu, P.; Kumar, R.; Tharmaraj, R.; Farooq Muhammad, U.; Pruncu, C. An experimental insight of friction stir welding of dissimilar AA 6061/Mg AZ 31 B joints. *Proc. Inst. Mech. Eng. Part B J. Eng. Manuf.* **2022**, *236*, 787–797. [CrossRef]
24. Rajendran, T.P.; Hynes, N.R.J.; Nikolova, M.P.; Christopher, T.; Danail, N. Influence of heat treatment on friction-welded joints made of high-carbon high-chromium tool steel/low-carbon steel for tooling applications. *J. Braz. Soc. Mech. Sci. Eng.* **2020**, *42*, 87. [CrossRef]
25. Rajesh Jesudoss Hynes, N.; Shenbaga Velu, P. Effect of rotational speed on Ti-6Al-4V-AA 6061 friction welded joints. *J. Manuf. Process.* **2018**, *32*, 288–297. [CrossRef]
26. Shenbaga Velu, P.; Rajesh Jesudoss Hynes, N.; Vignesh, N. J Influence of geometrical design on friction-welded AA6061/Ti6Al4V joints for wing spars of aircraft structures. *Surf. Rev. Lett.* **2022**, *29*, 2250076. [CrossRef]
27. Tharmaraj, R.; Rajesh Jesudoss Hynes, N. Investigation on the thermal behavior of friction stud welding of dissimilar aluminum/mild steel joints. *Surf. Rev. Lett.* **2022**, *29*, 2250093. [CrossRef]
28. Rajesh Jesudoss Hynes, N.; Shenbaga Velu, P. Microstructural and mechanical properties on friction welding of dissimilar metals used in motor vehicles. *Mater. Res. Express* **2019**, *6*, 026573. [CrossRef]
29. Hynes, N.R.J.; Velu, P.S.; Nithin, A.M. Friction push plug welding in airframe structures using Ti-6Al-4V plug. *J. Braz. Soc. Mech. Sci. Eng.* **2018**, *40*, 158. [CrossRef]
30. Hynes, N.R.J.; Nagaraj, P.; Sujana, J. Regression modelling of joining aluminium studs to steel with AA 1100 interlayer. *Exp. Tech.* **2019**, *43*, 491–500. [CrossRef]
31. Rajesh Jesudoss Hynes, N.; Vivek Prabhu, M.; Nagaraj, P. Joining of hybrid AA6063-6SiCp-3Grp composite and AISI 1030 steel by friction welding. *Def. Technol.* **2017**, *13*, 338–345. [CrossRef]
32. Tharmaraj, R.; Hynes, N.R.J.; Velu, P.S. Investigation on friction stud welded AMC/AISI 304 steel joints with ceramic intercoating. *J. Braz. Soc. Mech. Sci. Eng.* **2020**, *42*, 538. [CrossRef]
33. Velu, P.S.; Hynes, N.R.J.; Vignesh, N.J. Joining of AA 6061/Ti–6Al–4V with zinc interlayer using friction welding process. *J. Braz. Soc. Mech. Sci. Eng.* **2019**, *41*, 537. [CrossRef]
34. Seli, H.; Noh, M.Z.; Ahmad, A.I.; Endri, R.; Zainal, A.A. Characterization and thermal modelling of friction welded alumina-mild steel with the use of Al 1100 interlayer. *J. Alloys Compd.* **2010**, *506*, 703–709. [CrossRef]
35. Hynes, N.R.J.; Sankaranarayanan, R.; Tharmaraj, R.; Pruncu, C.I.; Dispinar, D. A comparative study of the mechanical and tribological behaviours of different aluminium matrix–ceramic composites. *J. Braz. Soc. Mech. Sci. Eng.* **2019**, *41*, 330. [CrossRef]
36. Nalbant, M.; Gokkaya, H.; Sur, G. Application of Taguchi method in the optimization of cutting parameters for surface roughness in turning. *Mater. Des.* **2007**, *28*, 1379–1385. [CrossRef]
37. Han, Q.; Viswanathan, S. Analysis of the mechanism of die soldering in aluminum die casting. *Metall. Mater. Trans. A* **2003**, *34*, 139–146. [CrossRef]